Supplemental Figure 1 (related to Figure 1)

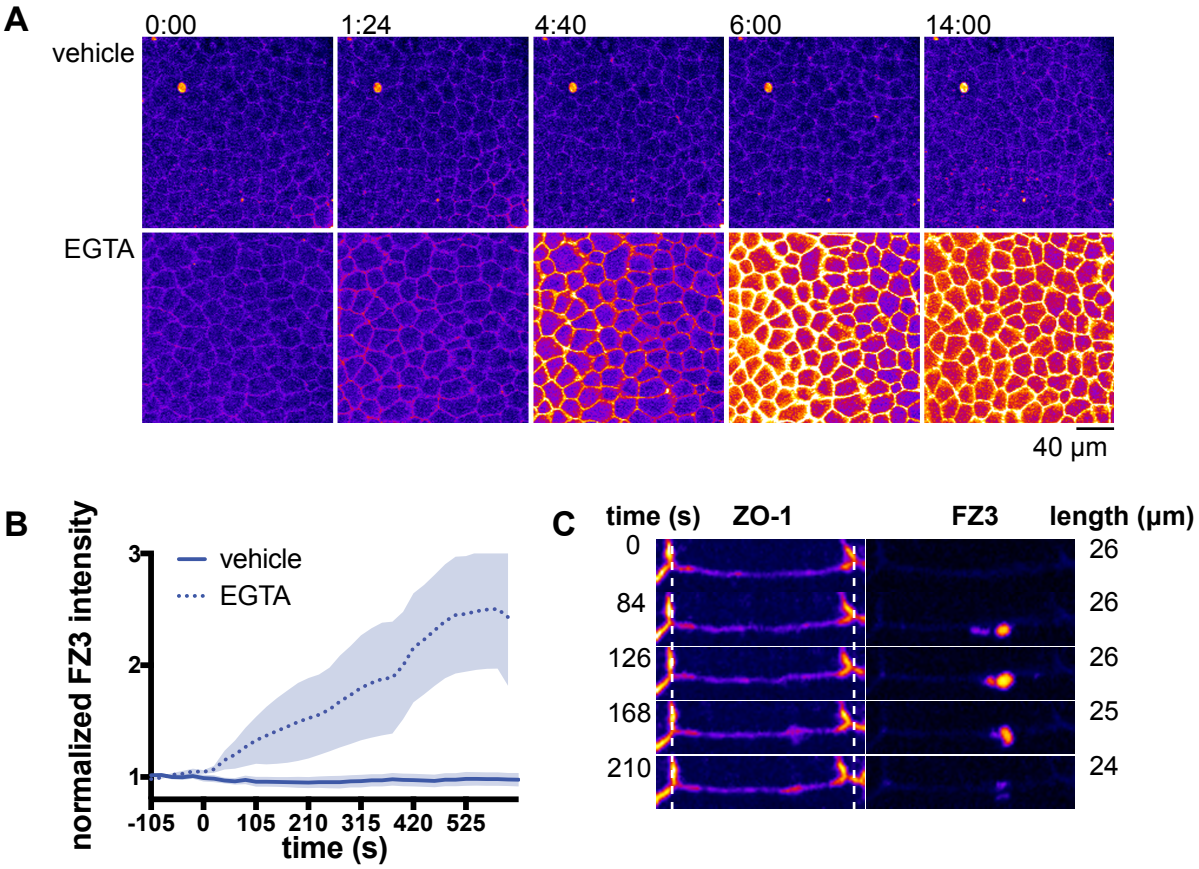

Figure S1. ZnUMBA detects global disruption of epithelial barrier function caused by EGTA. Related to Figure 1. a,b. Embryos were injected with FluoZin3. At time 0, a solution containing 2 mM ZnCl2 (vehicle) or 2 mM ZnCl2 + 10 mM EGTA (EGTA) was added to the imaging chamber during live imaging. FZ3 intensity increased globally in response to EGTA addition, which disrupts adherens and tight junctions. **a**. Increase in FZ3 intensity could be detected visually within two minutes of EGTA addition. Time is displayed as min:sec. **b**. Mean normalized FZ3 fluorescence intensity of a 456 µmx456 µm ROI normalized to mRFP-ZO-1 intensity in the same region. Shading represents S.E.M. Vehicle: n= 5,2 (embryos, experiments); EGTA: n=8,2. **c**. An example of junction contraction associated with resolution of a leak detected with FZ3 in the unperturbed *Xenopus laevis* epithelium. Dotted lines indicate the starting position of the vertices, and the junction length is displayed to the right.

Supplemental Figure 2 (related to Figure 2)

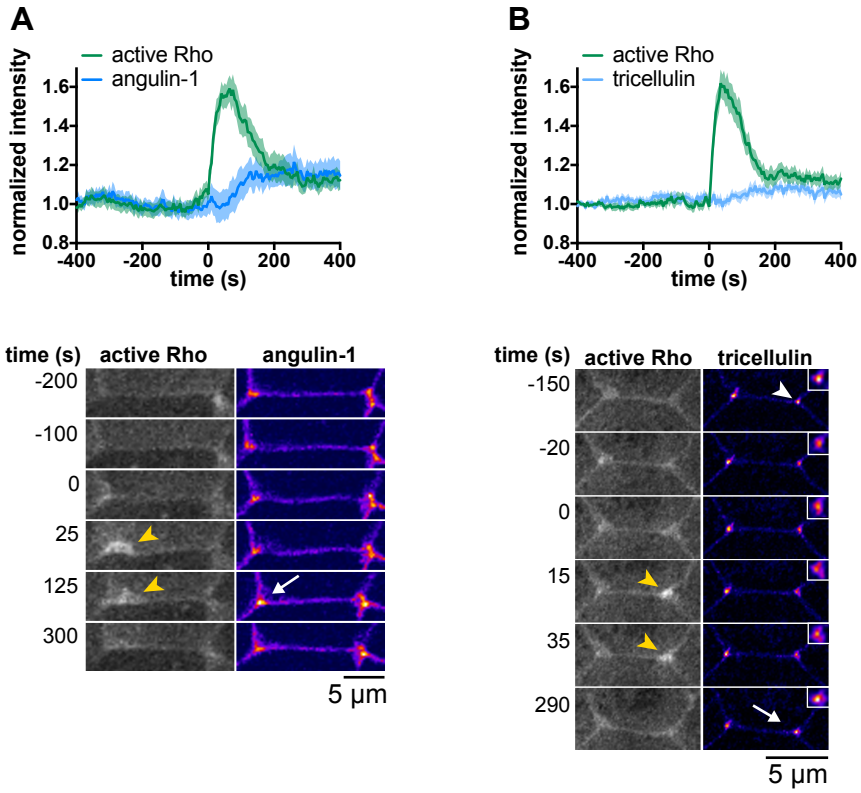

Figure S2. Rho flares remodel tricellular tight junctions. Related to Figure 2. Top: Mean normalized intensity of a region of interest encompassing the tricellular junction at the site of the flare over time. Shading represents S.E.M. **Bottom:** Co-imaging of Rho flares with tricellular tight junction (tTJ) proteins. Active Rho is shown in grey scale, angulin-1 and tricellulin shown with FIRE LUT. Yellow arrowheads indicate Rho flares, and white arrows indicate local protein increase. **a.** Angulin-1 does not decrease prior to Rho flares, although it is reinforced during flares. n=20,8,3 (flares, embryos, experiments); angulin-1-3xmCherry, GFP-rGBD. **b.** The intensity of tricellulin changes little over the course of the flare; however, the morphology of the tTJ is affected (see inset depicting the tTJ indicated by the white arrowhead). n=20,8,4. tricellulin-mCherry, GFP-rGBD.

Supplemental Figure 3 (related to Figures 2 and 3)

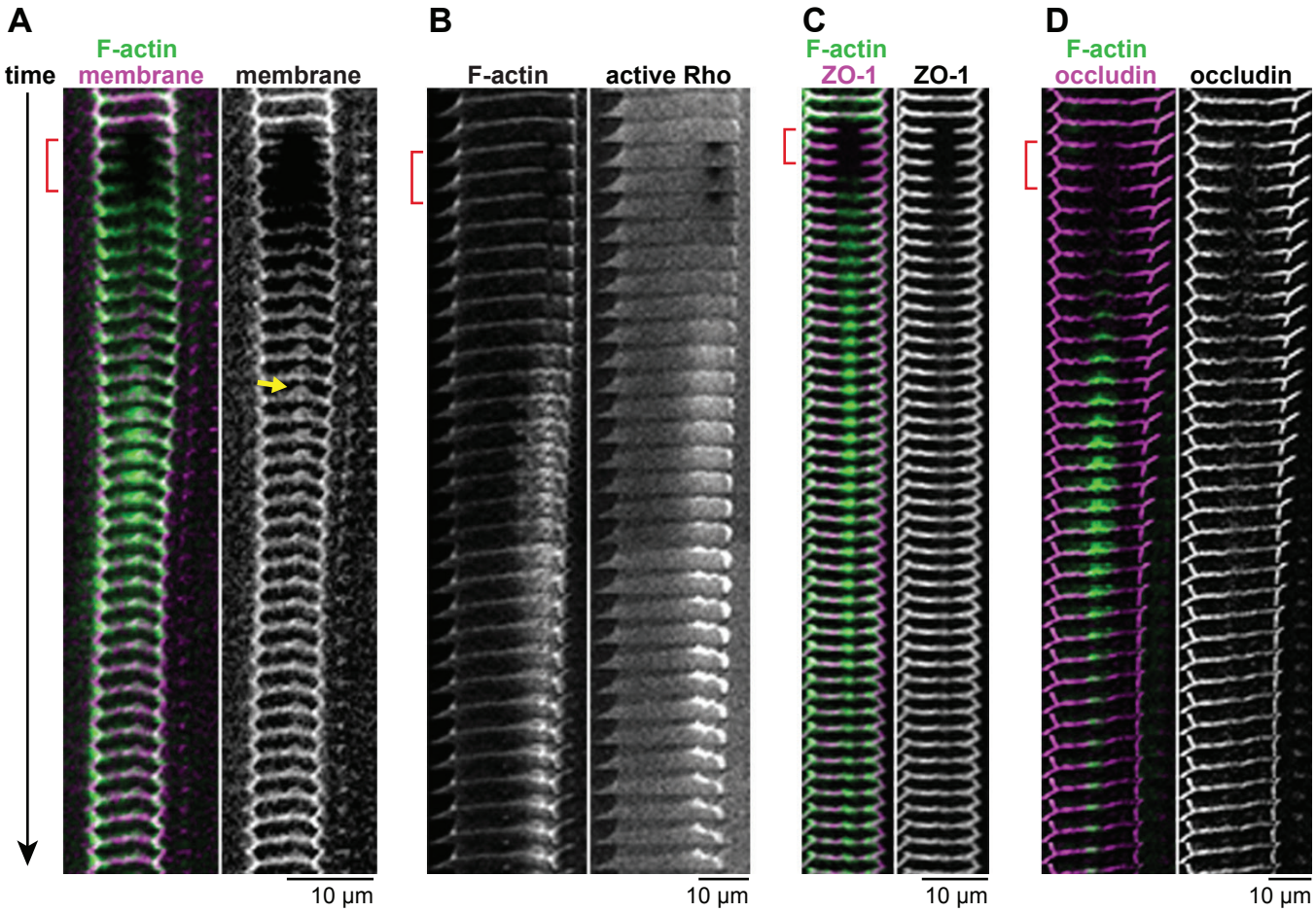

Figure S3. Laser injury recapitulates key aspects of Rho flare events. Related to Figures 2 and 3.
a. A 405 nm laser was activated in a small circular region on the junction to induce an injury (as in Fig 1b). Frames marked with red brackets indicate laser injury. Note that photobleaching accompanies injury. Junction injury results in protrusion of the plasma membrane (yellow arrow). F-actin: Lifeact-GFP, membrane: mCherry-farnesyl. **b.** Laser injury of the junction results in accumulation of active Rho (GFP-rGBD), which precedes F-actin (Lifeact-RFP) accumulation. **c,d.** Laser injury results in reinforcement of mRFP-ZO-1 (**c**) and mCherry-occludin (**d**). F-actin: Lifeact-GFP. Frames are 5 seconds apart.

Supplemental Figure 4 (related to Figure 5)

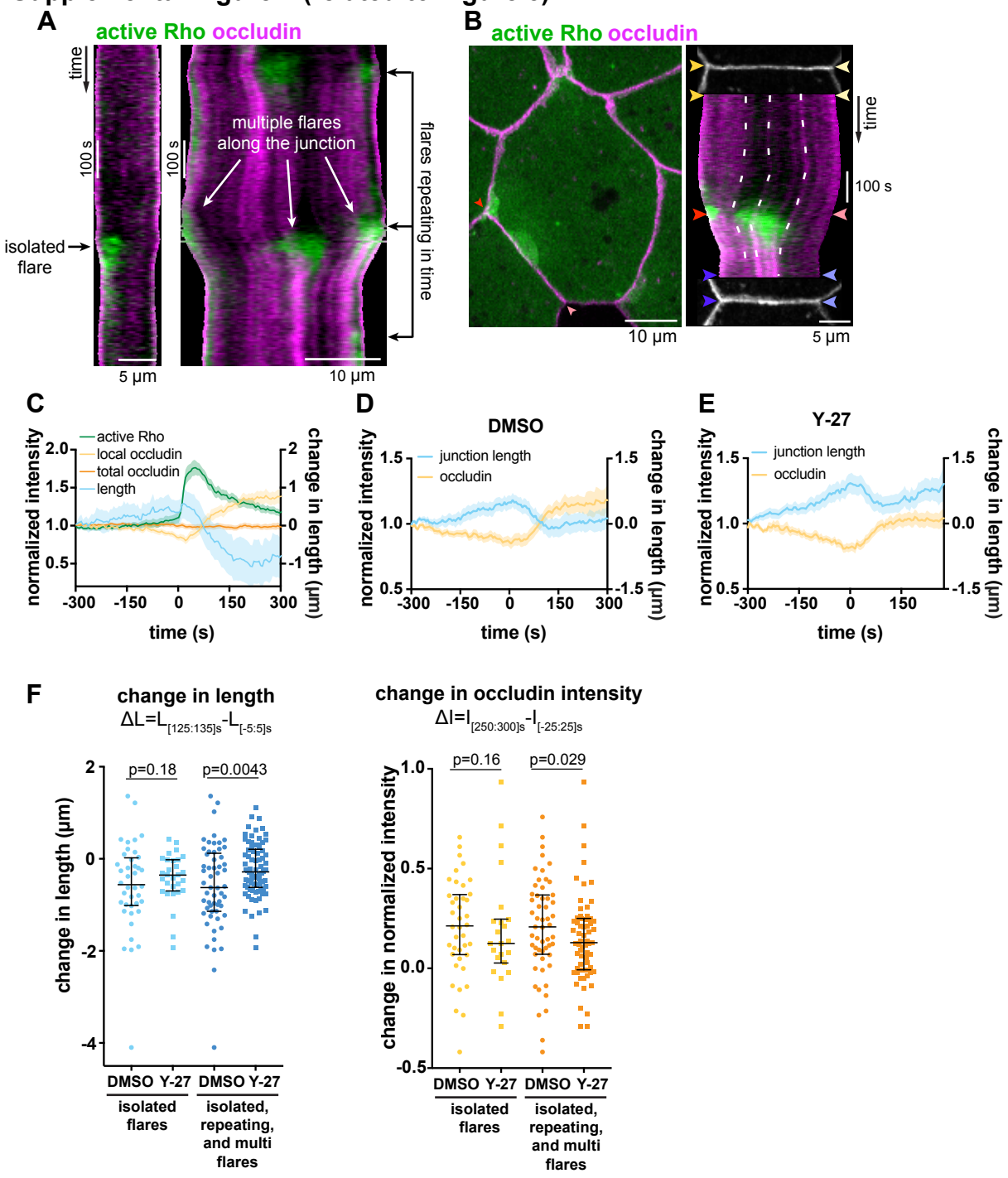

Figure S4. Junction contraction reinforces occludin. Related to Figure 5.
a. Kymographs of active Rho (GFP-rGBD, green) and occludin (mCherry-occludin, magenta) showing isolated and complex (repeating and multiple) flares. **b.** Occludin signal increases as the junction contracts locally. Color-coded arrowheads on the kymograph correspond to the timing of the images shown to the left, top, and bottom. Dashed white lines trace arbitrary fiducial marks in the kymograph, indicating distinct contractile units within the junction. **c.** Quantification of data from multiple kymographs. Time 0 corresponds to the start of the Rho flare. n=22,7,3 (flares, embryos, experiments) **d,e.** In isolated flares, ROCK inhibitor (Y-27632) did not significantly influence junction contraction relative to vehicle (DMSO), although elongation prior to the flare was increased. (**d**) n=40,8,3. (**e**) n=42,7,3 f. Change in junction length and occludin intensity was calculated from (**d,e**) for isolated flares. When complex flares were considered in addition to isolated flares, both contraction and occludin reinforcement are significantly reduced. DMSO: n=58,8,3 (note: one outlier was omitted from the DMSO plot: ΔL=-0.95, ΔI=3.14); Y-27632: n=99,7,3. P-values were calculated using Mann-Whitney *U* test.

Supplemental Figure 5 (related to Figure 6)

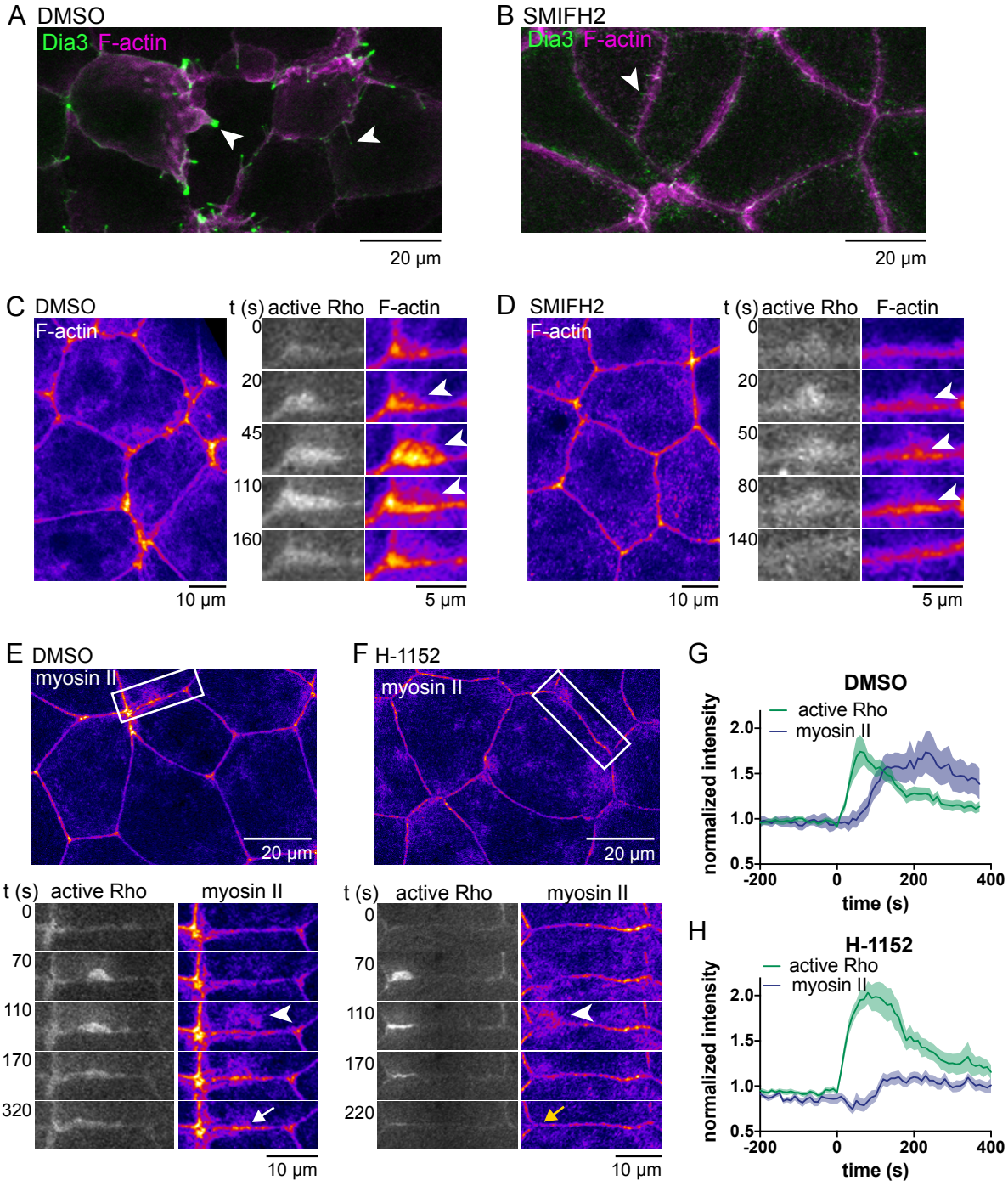

Figure S5. Effect of SMIFH2 and H-1152 on F-actin and myosin II accumulation at Rho flares. Related to Figure 6. **a.** 3xGFP-Dia3 expression induces actin-rich filopodia-like protrusions (white arrowheads). **b.** SMIFH2, a formin inhibitor, reduces the size and dynamics of these protrusions. **c,d.** SMIFH2 treatment reduces, but does not completely inhibit actin polymerization (white arrowheads) at Rho flares. GFP-rGBD, Lifeact-RFP. **e-h.** H-1152, a ROCK inhibitor, reduces myosin II accumulation at junctions following Rho flares. **e,f.** Live imaging of active Rho and myosin II in the presence of DMSO or H-1152. While the halo of myosin II still appears at the periphery of the flare during both DMSO and H-1152 treatment (white arrowheads), it fails to coalesce at the junction during H-1152 treatment (white arrow vs yellow arrow). **g,h.** Quantification of active Rho and myosin II accumulation at the junction during Rho flares. SF9-mNeon, mChe-2xrGBD. DMSO: n=19,6,3 (flares, embryos, experiments); H-1152: n=23,9,3.